Supporting Information

Modulating Polymorphic Phase Boundaries and Defect Chemistry in KNN-Based Piezoceramics Through Multi-Element Doping Strategies

Mrinmoy Brahma[1], Md Shafayatul Islam[2], Mehedi Hasan Prince[3], S M Khalid Hossain[1], Md Shofiqul Islam[4], Aninda Nafis Ahmed[4*], Sheikh Manjura Hoque[5], Ahmed Sharif[1*]

[1]Department of Materials and Metallurgical Engineering, Bangladesh University of Engineering and Technology, Dhaka 1000, Bangladesh.

[2]Department of Materials Science and Engineering, University of Illinois Urbana Champaign, Urbana, Illinois, 61801, USA.

[3]Department of Materials Science & Engineering, Rensselaer Polytechnic Institute (RPI), NY, 12180, USA.

[4]Pilot Plant and Process Development Centre, Bangladesh Council of Scientific and Industrial Research, Dhaka, Bangladesh.

[5]Materials Science Division, Atomic Energy Centre, Dhaka, Bangladesh.

*Corresponding Author's Email: asharif@mme.buet.ac.bd (Dr. Ahmed Sharif) and adhi88bd@yahoo.com (Dr. Aninda Nafis Ahmed)

XRD:

Table S1 Crystal cell parameters of Pure-KNN, KNN-BiLaTi, and KNN-LaYVSb ceramics.

Sample	Pure KNN	KNN-BiLaTi	KNN-LaYVSb
Unit cell parameter	a = 3.948 b = 5.599 c = 5.636 α = β = γ = 90° V = 124.59	a = 3.934 b = 5.562 c = 5.622 α = β = γ = 90° V = 123.00	a = 3.934 b = 5.562 c = 5.622 α = β = γ = 90° V = 123.00

Table S2 Density calculation of Pure-KNN, KNN-BiLaTi, and KNN-LaYVSb ceramics.

Sample	$\rho_{apparent}$ [g/cm^3]	$\rho_{x\text{-}ray}$ [g/cm^3]	$\rho_{relative}$ [%]
Pure KNN	4.11	4.64	88.58
KNN-BiLaTi	4.22	4.98	84.74
KNN-LaYVSb	4.30	4.68	91.88

The densification of the ceramics was assessed by comparing the experimentally measured apparent densities with the theoretical densities derived from X-ray data. The calculated relative

densities summarized in Table S2 reveal that pure KNN attains 88.58% densification. A clear compositional dependence is observed upon doping that LaYVSb-doped KNN exhibits an enhanced relative density of 91.88%, suggesting improved densification and reduced porosity, while BiLaTi-doped KNN exhibits reduced densification of 84.74%, likely due to enhanced porosity. This indicates that dopant chemistry plays a critical role in governing sintering behavior and final microstructural density.

XPS:

Fig. S1 shows the deconvoluted O 1s core-level spectra of pure KNN, which reveals three distinct peaks: lattice oxygen (O_L) around ~529 eV, oxygen vacancies (O_V) near ~531 eV, and surface-adsorbed hydroxyl-like oxygen (O-H) approximately ~532 eV [1]. The dominance of the OL peak confirms that oxygen primarily exists in the well-bonded Nb-O bond in the orthorhombic KNN lattice. O_V indicates the presence of some oxygen vacancies, and the small high-energy shoulder represents the O-H bond that may come from surface contamination, which is common in air-

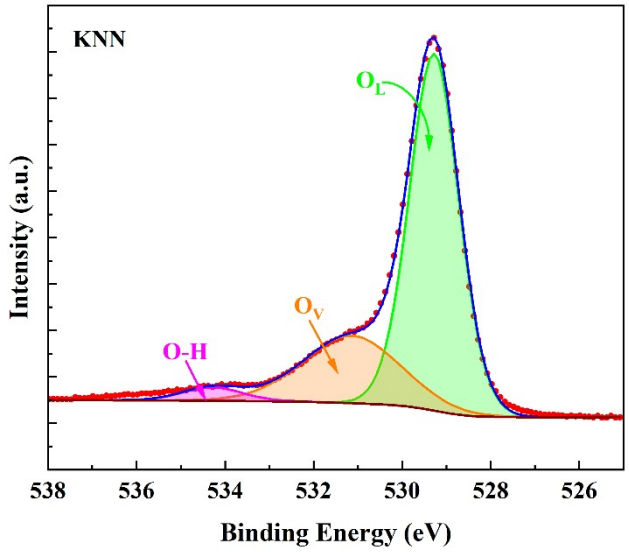

Fig. S1 High-resolution XPS spectra of O 1s, displaying lattice oxygen (O_L), oxygen vacancy (O_V) contribution and oxygen from O-H-like bond, from KNN.

exposed oxygen ceramics.

Fig. S2 displays the O 1s, Bi 4f, La 4d, and Ti 2p core-level spectra for the KNN-BiLaTi sample. Compared to KNN, there is a slight shift to higher binding energy in the O 1s peak, indicating a modification in the Nb-O bonding caused by the doping of Bi, La, and Ti. This shift reflects the

development of local lattice strain, which is also supported by the Raman data and aligns with some previous studies [2]. The Bi 4f spectrum features two distinct peaks at approximately ~ 159 eV (Bi $4f_{7/2}$) and ~ 164 eV (Bi $4f_{5/2}$), confirming the +3 oxidation state of Bi [3]. The presence of La $3d_{3/2}$ and La $3d_{5/2}$ peaks at ~105 eV and ~102 eV, respectively, confirms the presence of La3+, which bonds to oxygen atoms in the perovskite structure [4]. The Ti signal appears as a single well-defined Ti 2p peak at approximately 458 eV, consistent with the Ti^{4+} oxidation state [5].

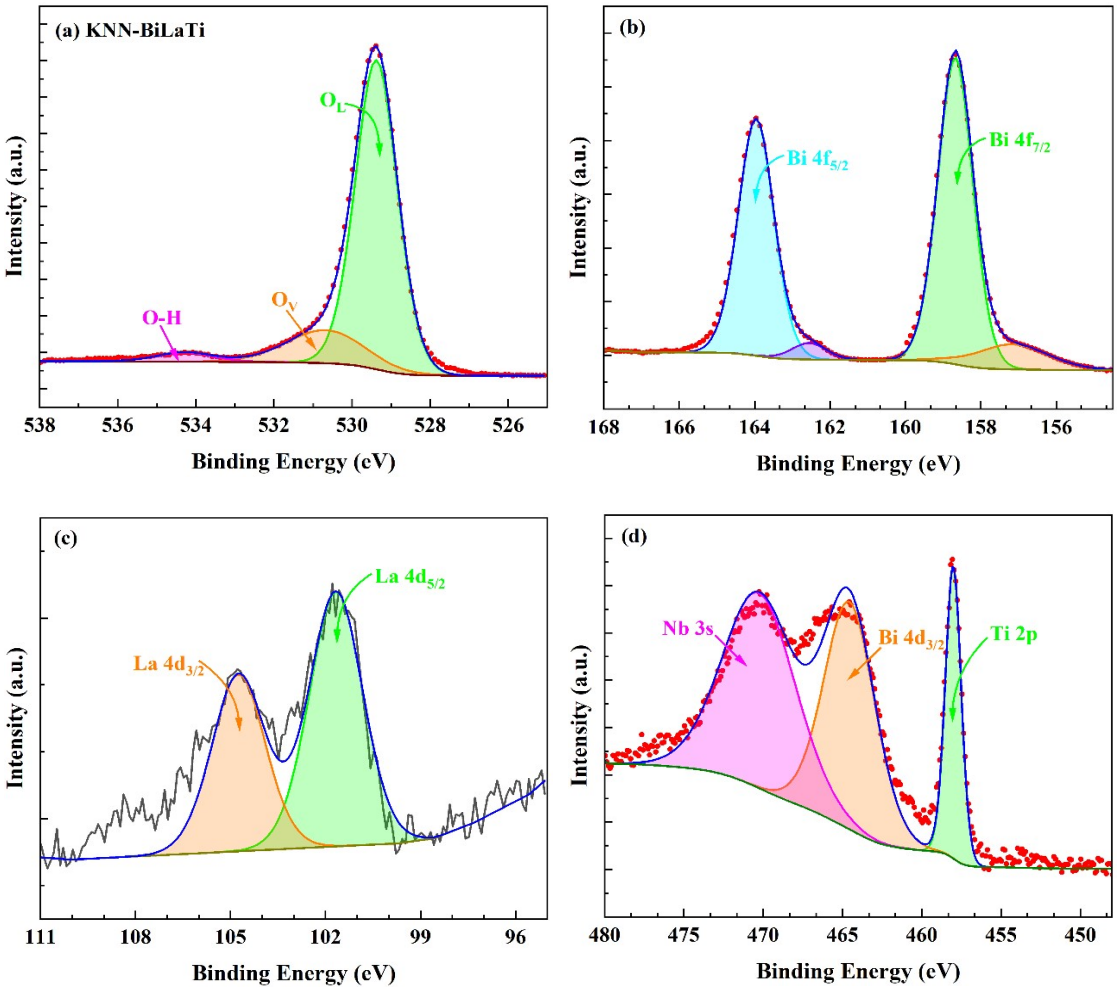

Fig. S2 XPS core level spectra for O 1s, Bi 4f, La 4d and Ti 2p in KNN-BiLaTi sample. (a) O1s spectra (b) Bi 4f spectra showing peaks corresponding to Bi $4f_{7/2}$ and Bi $4f_{5/2}$ states. (c) La 4d spectra displaying the La $4d_{3/2}$ and La $4d_{5/2}$ peaks. (d) Ti 2p spectra along with Bi $4d_{3/2}$ and Nb 3s peaks.

Fig. S3 displays the deconvoluted spectra for the O 1s, Sb 3d, La 4d, and Y 3d regions obtained from KNN-LaYVSb. The O_L and O_V peaks resemble those of KNN-BiLaTi; however, a slight increase in the O_V suggests a higher amount of oxygen vacancies in this sample. This aligns with

the higher lattice distortion, which correlates with improved piezoelectric coefficients. The Sb $3d_{5/2}$ (~530 eV) and Sb $3d_{3/2}$ (~539 eV) peaks confirm the presence of the Sb^{5+} oxidation state [6]. The V $2p_{3/2}$ (~516 eV) and V $2p_{1/2}$ (~524 eV) peaks correspond to the V^{5+} state [7]. These high-valent cations (V, Sb) occupy the B-site, promoting charge balance and stabilizing the perovskite structure. The La 4d doublet remains consistent with the KNN-BiLaTi sample, which is La^{3+}, while Y $3d_{5/2}$ and Y $3d_{3/2}$ peaks at 157 eV and 159 eV confirm the Y^{3+} oxidation state [8].

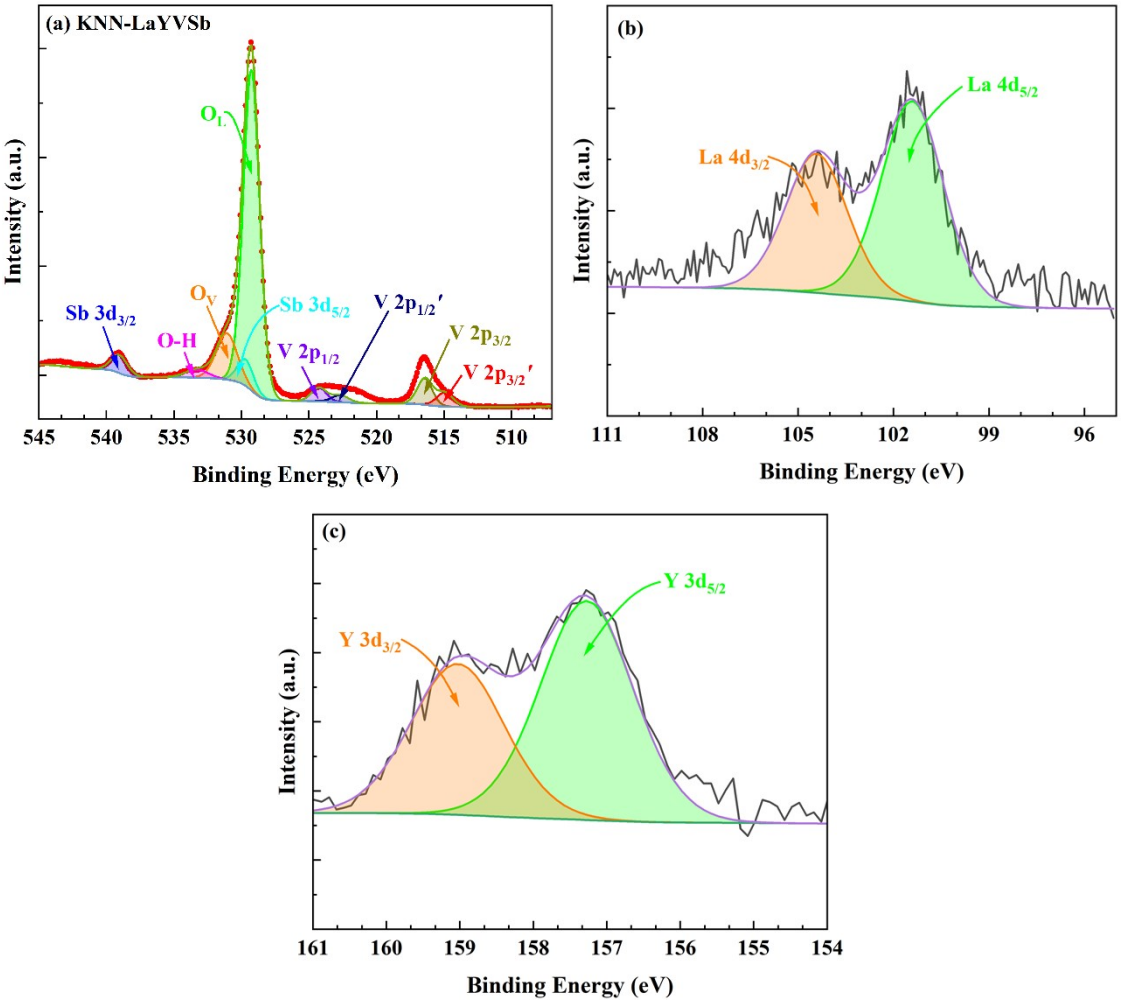

Fig. S3 Core-level XPS spectra of KNN-LaYVSb (a) O1s, Sb3d and V2p region, showing peaks from Sb $3d_{5/2}$ and Sb $3d_{3/2}$ states along with V $2p_{3/2}$, V $2p_{1/2}$, and (b) La 4d spectra displaying the La $4d_{3/2}$ and La $4d_{5/2}$ peaks; (c) Y 3d region, showing peaks corresponding to Y $3d_{3/2}$ and Y $3d_{5/2}$.

SEM:

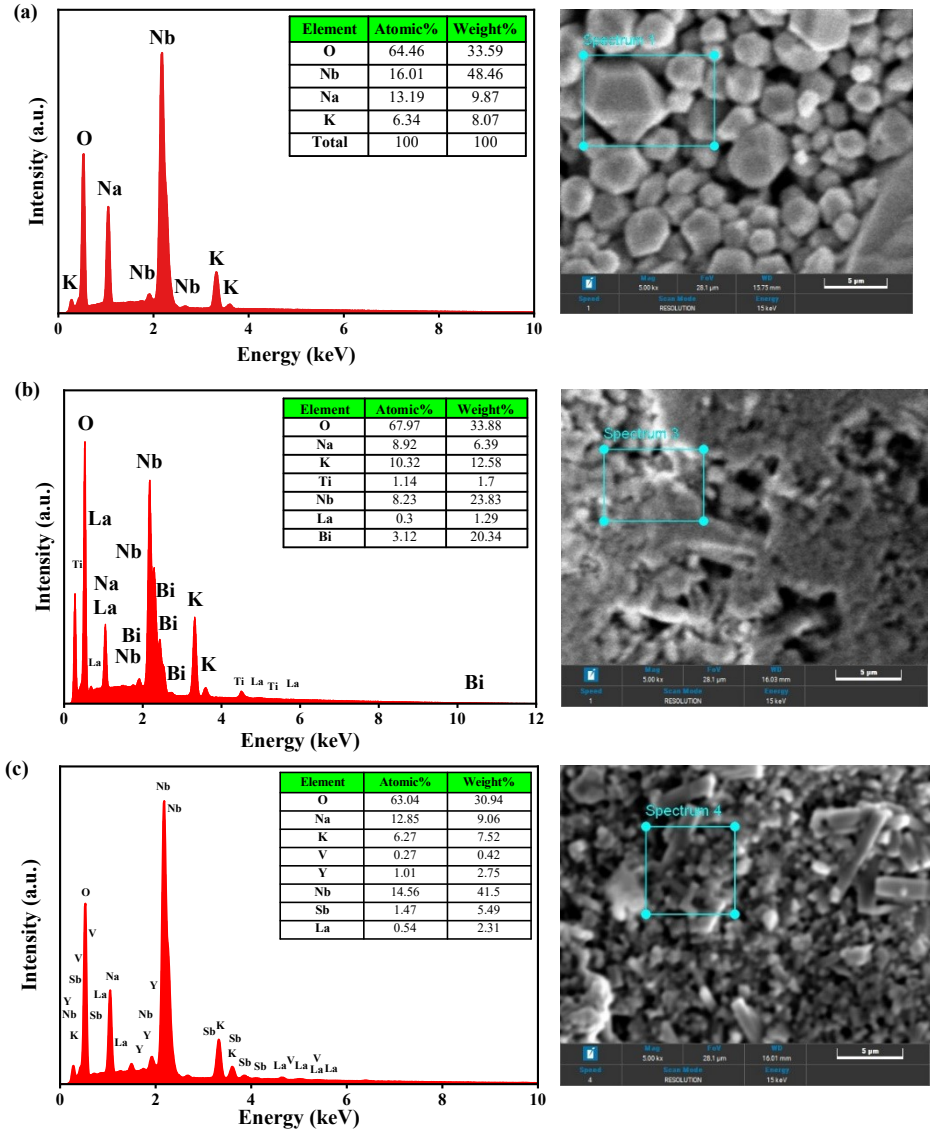

Fig. S4 Elemental analysis by EDS (a) Pure-KNN, (b) KNN-BiLaTi, (c) KNN-LaYVSb

Hysteresis Loops:

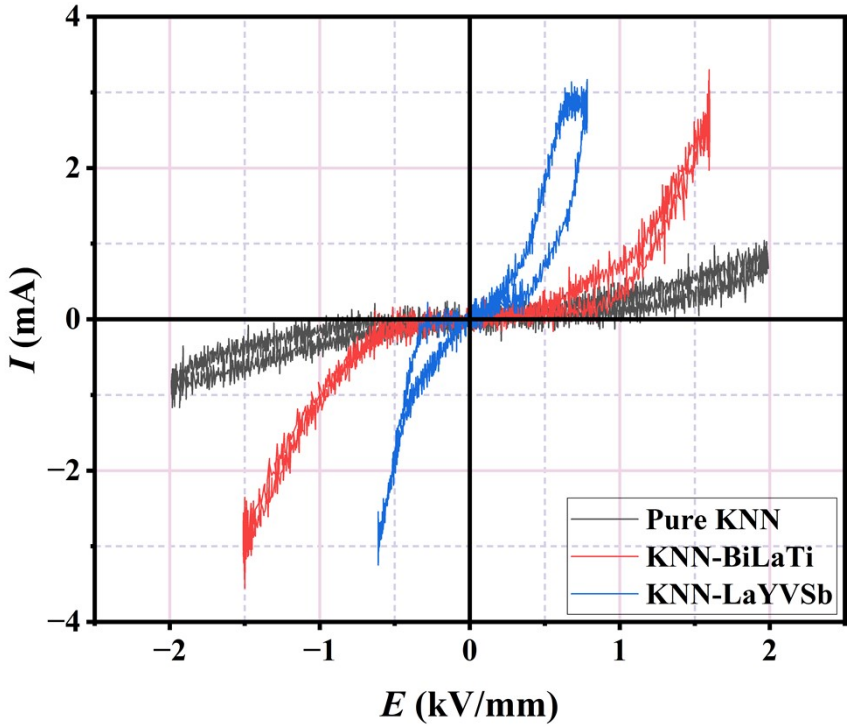

Fig. S5 Room temperature instantaneous current vs. electric field (I-E) plots of Pure-KNN, KNN-BiLaTi, and KNN-LaYVSb ceramics obtained at 50 Hz.

The corresponding instantaneous current vs. electric field (I-E) curves obtained during the P-E loop experiments are displayed in Fig. S5. For KNN-BiLaTi and KNN-LaYVSb in particular, a noticeable rise in current is seen in the high-field region, suggesting an increased non-switching current contribution at higher applied fields. Similar high-field conduction behavior has been described in KNN-based ferroelectrics, where leakage current could restrict full loop saturation [9], [10], [11]. Therefore, further increase of the electric field was avoided, as it would reduce the reliability of the obtained polarization data and raise the probability of electrical failure under the present measurement conditions. As demonstrated in Table S2, variances in relative density exist across the samples; yet, the current response in Fig. S5 does not correlate with density alone, indicating that compositional and defect-related factors also contribute.

REFERENCES:

[1] J.-Y. Park, I.-R. Yoo, S.-H. Choi, and K.-H. Cho, "Volatilization of Alkali Elements during the Potassium Sodium Niobate Thin Film Deposition Process via RF Magnetron Sputtering," *Korean. J. Mater. Res.*, vol. 35, no. 2, pp. 82–89, Feb. 2025, doi: 10.3740/MRSK.2025.35.2.82.

[2] A. Chauhan *et al.*, "Phase transition, microstructural evolution, and neurotoxicity of Gd-doped sodium potassium niobate nanoparticles in zebrafish models," *Inorganic Chemistry Communications*, vol. 182, p. 115357, Dec. 2025, doi: 10.1016/j.inoche.2025.115357.

[3] F. Wang *et al.*, "Oxygen vacancies induced by zirconium doping in bismuth ferrite nanoparticles for enhanced photocatalytic performance," *Journal of Colloid and Interface Science*, vol. 508, pp. 237–247, Dec. 2017, doi: 10.1016/j.jcis.2017.08.056.

[4] M. Uma *et al.*, "Structural, Chemical and Electrical Properties of Au/La2O3/n-GaN MIS Junction with a High-k Lanthanum Oxide Insulating Layer," *Journal of Elec Materi*, vol. 48, no. 7, pp. 4217–4225, Jul. 2019, doi: 10.1007/s11664-019-07193-8.

[5] N. Kitchamsetti *et al.*, "An Investigation on the Effect of Li–Ion Cycling on the Vertically Aligned Brookite TiO_2 Nanostructure," *ChemistrySelect*, vol. 4, no. 21, pp. 6620–6626, Jun. 2019, doi: 10.1002/slct.201900395.

[6] E. R. Cleveland, L. B. Ruppalt, B. R. Bennett, and S. M. Prokes, "Effect of an in situ hydrogen plasma pre-treatment on the reduction of GaSb native oxides prior to atomic layer deposition," *Applied Surface Science*, vol. 277, pp. 167–175, Jul. 2013, doi: 10.1016/j.apsusc.2013.04.018.

[7] H. T. T. Nguyen, D. Jung, C.-Y. Park, and D. J. Kang, "Synthesis of single-crystalline sodium vanadate nanowires based on chemical solution deposition method," *Materials Chemistry and Physics*, vol. 165, pp. 19–24, Sep. 2015, doi: 10.1016/j.matchemphys.2015.05.053.

[8] L. Mariscal-Becerra, R. Vázquez-Arreguín, U. Balderas, S. Carmona-Téllez, H. Murrieta Sánchez, and C. Falcony, "Luminescent characteristics of layered yttrium oxide nano-phosphors doped with europium," *Journal of Applied Physics*, vol. 121, no. 12, p. 125111, Mar. 2017, doi: 10.1063/1.4979209.

[9] L. Wang, W. Ren, P. Shi, and X. Wu, "Structures, electrical properties, and leakage current behaviors of un-doped and Mn-doped lead-free ferroelectric K0.5Na0.5NbO3 films," *J. Appl. Phys.*, vol. 115, no. 3, p. 034103, Jan. 2014, doi: 10.1063/1.4861415.

[10] R. Pinho *et al.*, "Stress induced effects on piezoelectric polycrystalline potassium sodium niobate thin films," *Journal of Materials Chemistry C*, vol. 11, no. 23, pp. 7758–7771, 2023, doi: 10.1039/D2TC05538D.

[11] H. Deng *et al.*, "Orientation dependence of electrical properties of large-sized sodium potassium niobate lead-free single crystals," *CrystEngComm*, vol. 16, no. 13, pp. 2760–2765, Mar. 2014, doi: 10.1039/C3CE42464B.